International Journal of Adhesion & Adhesives 52 (2014) 11–18

Contents lists available at ScienceDirect

International Journal of Adhesion & Adhesives

journal homepage: www.elsevier.com/locate/ijadhadh

Isothermal epoxy-cure monitoring using nonlinear ultrasonics

V. Koissin [a,1], A. Demčenko [a,*], V.A. Korneev [b]

[a] Faculty of Engineering Technology, University of Twente, 7500AE Enschede, The Netherlands
[b] Lawrence Berkeley National Laboratory, Berkeley, CA, United States

ARTICLE INFO

Article history:
Accepted 2 January 2014
Available online 25 February 2014

Keywords:
Epoxy
Cure kinetics
Nonlinear ultrasonics
Calorimetry
Rheometry
Glass transition
Vitrification

ABSTRACT

Isothermal curing of LY 1564SP resin in an aluminium-adhesive-aluminium laminate is investigated, using a nonlinear ultrasonic immersion technique, to prove its applicability for this type of dynamic material transformation. For verification and comparison, epoxy-cure kinetics and rheological behavior are measured using differential scanning calorimetery (DSC) and dynamic mechanical analysis (DMA). Results reveal that the nonlinear ultrasonics, based on noncollinear wave mixing, can successfully be applied to in situ epoxy-cure monitoring—for example, to adhesive bonds—with reliable detection of gelation and vitrification time instants.

1. Introduction

Ultrasonic measurements are widely used to detect dynamic changes and transition points in polymer materials. For example, they are successfully employed to monitor solidification and shrinkage processes [1,2], polymerization [3], physical ageing [4], and epoxy cure [5–8]. The main advantages of the ultrasonic techniques include relatively low cost, high sensitivity, and in-line and real-time measurement possibilities. The curing processes inherent for epoxy resins are the practically important example, because measuring the cure characteristics helps to develop an optimal cure process, which would achieve the best material performance. The use of ultrasonics also enables real-time quality control. The reported results demonstrate that ultrasonic measurements, which employ longitudinal and/or shear waves, are applicable for monitoring of thin epoxy layers [8–14] and for detection of gelation time when a viscous epoxy transforms into an elastic gel [5,7,15–20].

Nonlinear ultrasonics can often be more sensitive to material properties than linear ultrasonics. Historically, nonlinear ultrasonics usually employs a multiple harmonic generation of a single monochromatic wave, rather than other nonlinear measurement techniques. These harmonic generation measurements are relatively easy to implement. However, data from such measurements can be difficult to interpret, because of similar nonlinearity effects occurring in an acoustic channel, electronics, or a surrounding medium that masks a target signal. Fortunately, one wave-mixing technique [21] is free of these disadvantages, allowing for easy frequency-domain separation of a target sum and/or difference frequencies generated in the specimen from the multiples generated by other sources. Moreover, this wave-mixing technique, in its noncollinear form (when the primary beams interact at non-zero angles), further improves detection of the target waves, because such waves are also separated in space from other signals.

Despite the high potential of noncollinear wave mixing for nondestructive testing applications, noncollinear wave mixing is still not verified well enough for epoxy-cure monitoring. Also, there is at this time insufficient information about ultrasonic detection of the vitrification time (i.e., when the mobility of reactive groups vanishes and the epoxy undergoes a rubber-glass transition, then quickly approaches a solid state [22]). In this paper, we present an experimental study aiming at a partial filling of this knowledge gap. The presented nonlinear elastic wave-mixing technique enables monitoring of the epoxy cure in a thin layer (about 0.2 mm thick), with a robust detection of the characteristic points (gelation and vitrification). The importance of this method is illustrated, showing that the nonlinear-elastic material response has a higher sensitivity to the epoxy rheology compared to the linear response. Independent verifications are performed, with commonly used rheometry (dynamic mechanical analysis, DMA) and differential scanning calorimetry (DSC) measurements of the isothermal epoxy cure. Finally, the advantages and disadvantages of the three methods are compared.

* Corresponding author.
E-mail address: andriejus.demcenko@gmail.com (A. Demčenko).
[1] Present address: Composites Research Unit, Department of Mechanical Engineering, University of Bath, BA2 7AY, UK.

http://dx.doi.org/10.1016/j.ijadhadh.2014.01.003
0143-7496 © 2014 Published by Elsevier Ltd.

2. Noncollinear ultrasonic wave mixing

In isotropic nonlinear materials (described with the third-order elastic constants *l,m,n* [21]), the *resonant conditions* might exist wherein two elastic waves could possibly interact to generate scattered waves with mixed (sum and difference) frequencies. These conditions are

$$\omega_r = \omega_1 \pm \omega_2, \tag{1}$$

$$\mathbf{k}_r = \mathbf{k}_1 \pm \mathbf{k}_2, \tag{2}$$

where frequencies ω_1, ω_2, and ω_r represent two initial waves and the resonant wave, respectively. The parameters $\mathbf{k}_1$, $\mathbf{k}_2$, and $\mathbf{k}_r$ are their wave vectors. Even if the resonant conditions were satisfied, the scattered wave amplitude can be zero for all parameter combinations (polarization restriction). In [21], it is shown that only 10 of 54 possible combinations of two initial compressional L, and/or shear SV, and/or shear SH waves generate scattered resonance waves.

Two wave interaction cases

$$\mathrm{SV}(\omega_1)+\mathrm{L}(\omega_2)\rightarrow \mathrm{L}(\omega_1+\omega_2), \tag{3}$$

$$\mathrm{SV}(\omega_1)+\mathrm{SV}(\omega_2)\rightarrow \mathrm{L}(\omega_1+\omega_2), \tag{4}$$

appear to be the most suitable for nondestructive testing purposes [23]. These interactions can be used in single-sided or double-sided-access measurement modes (see Fig. 1), using either contact or immersion ultrasonic measurement techniques. This property enables us to find incident angles of primary waves such that the generated longitudinal wave strikes the specimen/liquid interface perpendicularly. This perpendicular incidence also allows us to achieve the highest energy rate for the nonlinear wave and helps to simplify the acoustic channel, because there is no need to rotate the receiver at a specific angle.

Fig. 1 shows a submerged wave-mixing technique scheme with two modifications, using either reflected or transmitted scattered waves. For thick objects, the transmitted wave might be preferred, because the target scattered wave has a shorter path (i.e., less attenuation) and can be detected more readily. The advantage of the reflected wave scheme is in its single-side access to the specimen.

Interaction $\mathrm{SV}(\omega_1)+\mathrm{SV}(\omega_2)\rightarrow \mathrm{L}(\omega_1+\omega_2)$ between two shear waves appears most promising, because in this case it maintains a wave mode separation. However, this interaction requires a large angle between the two interacting waves (usually more than 120°). Therefore, it cannot be used for materials having low ultrasonic wave velocities; a conventional immersion measurement technique should be employed instead. This angle restriction can be overcome, however, by employing the interaction $\mathrm{SV}(\omega_1)+\mathrm{L}(\omega_2)\rightarrow \mathrm{L}(\omega_1+\omega_2)$ between shear and longitudinal waves. Note that

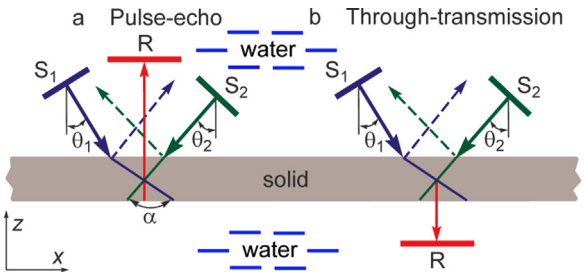

Fig. 1. Pulse-echo and through-transmission arrangement of transducers for single-side and double-side access measurements. Shown are the scattered wave receiver R, the pump wave sources $S_{1,2}$ having inclination angles $\theta_{1,2}$, respectively. α is the wave interaction angle. Red lines show propagation paths of the resonant wave. Dashed lines mark the specularly reflected pump waves. (For interpretation of the references to color in this figure legend, the reader is referred to the web version of this article.)

both chosen interactions are the functions of one third-order elastic constant m only, as illustrated in Table 2 in [21]. Imaging and testing of two other elastic constants, l and n, require other interactions.

The interaction (4) between two shear waves was employed for the epoxy-cure monitoring. The corresponding nonlinear wave amplitude coefficient (with dimension length^{-3}) is [21]

$$W = D_L\frac{1+d}{2\gamma^2}[C_1\ \cos\ 2\alpha + C_2\cos^2\alpha - C_3\sin^2\alpha] \approx D_L\frac{1+d}{2\gamma^2}m\ \cos\ 2\alpha, \tag{5}$$

where the following notations are used:

$$D_L = d/(4\pi c_L^2\rho)(\omega_1/c_r)^3, \tag{6}$$

$$\gamma = c_S/c_L, \tag{7}$$

$$d = \omega_2/\omega_1. \tag{8}$$

Parameter α is the wave interaction angle, c_L and c_S are the longitudinal and shear wave velocities in a medium, respectively, ρ is the material density, and c_r is the nonlinear wave velocity in a medium (in our case $c_r = c_L$). The constants C_i have simple relations:

$$C_1 = \mu+\frac{A}{4},\quad C_2 = \lambda+\mu+\frac{A}{4}+B,\quad C_3 = \frac{A}{4}+B,\quad C_4 = B+2C,$$
$$C_5 = \lambda+B, \tag{9}$$

with third-order elastic constants and Lamé parameters λ and μ. Prediction of the nonlinear wave amplitude coefficient enables us to choose the measurement conditions under which the highest nonlinear wave amplitude is expected, and maintains the best signal-to-noise ratio. Note that the nonlinear wave amplitude coefficient has a dependence on the ω_1^3 (see Eq. (5)), indicating that the noncollinear wave interaction is more strongly pronounced at higher frequencies.

An example of a nonlinear wave amplitude calculation is shown in Fig. 2 for aluminium studied in [24]; its properties are listed in Table 1.

Prediction of the nonlinear wave amplitude is carried out when attenuation is not taken into account and ω_1 is 4 MHz. Fig. 2a shows the predicted nonlinear wave amplitude coefficient W (red curve), the nonlinear wave scattering angle ψ (blue curve), and the wave interaction angle α (black curve) over the entire allowed frequency range [21]. The scattering angle ψ is calculated between the first pump-wave vector of frequency ω_1 and the nonlinear wave vector [21]. When ultrasonic experiments are performed using the immersion technique, it is useful to employ a procedure that allows tuning an acoustical channel for noncollinear wave mixing [23]. The optimized parameters (the nonlinear wave amplitude coefficient W_T, and the inclination angles θ_1 and θ_2 for the pump-wave sources) when the nonlinear wave strikes the aluminium/water interface perpendicularly for the through-transmission mode are shown in Fig. 2b. W_T is the nonlinear wave-amplitude coefficient when the energy-transmission coefficients between the liquid–solid (T_1 and T_2), and the solid–liquid (T) interfaces are taken into account. Therefore, the amplitude function is $W_T = W\times T_1\times T_2\times T$ — presented in [23] in detail.

As seen in Fig. 2, the predicted maximum of the nonlinear wave amplitude coefficient in the frequency ratio range 0.6–1.66 is shifted from the initial frequency ratio ($d=1.56$, Fig. 2a) to the frequency ratio $d=1.32$. This shift occurs because of the energy transmission and reflection coefficient between the water–aluminium and aluminium–water interfaces.

Since commercially available ultrasonic transducers of standard frequencies are available, it is practical to choose the frequency ratio of pump (primary) waves in such a way that both the performance of the transducers and the sensitivity of the receiver to the

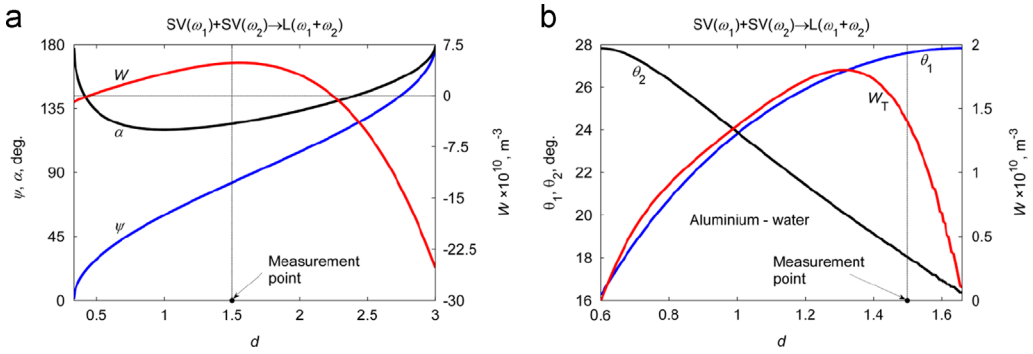

Fig. 2. Predicted nonlinear wave amplitude coefficient W versus frequency ratio d for SV(ω_1)+SV(ω_2)→L($\omega_1+\omega_2$) wave mixing in aluminium (a); where α is the wave interaction angle and ψ is the resonant wave propagation angle. (b) Shows the optimized parameters when the nonlinear wave strikes the aluminium/water interface perpendicularly. W_T is the nonlinear wave amplitude coefficient when the energy transmission coefficients between interfaces (water–aluminium and aluminium–water) are taken into prediction account. Also shown are inclination angles θ_1 and θ_2 for the pump waves. (For interpretation of the references to color in this figure, the reader is referred to the web version of this article.)

Table 1
Material properties used in the nonlinear wave analysis.

Material	λ, GPa	μ, GPa	l, GPa	m, GPa	n, GPa	ρ, kg/m^3
Aluminium	54.308	27.174	−281.5	−339	−416	2704

nonlinear wave stay high. With this in mind, we set the frequency ratio ω_2/ω_1 to 1.5, and the corresponding frequencies of the pump waves to 6 MHz and 4 MHz, respectively (see Fig. 2). A nonlinear wave of a 10 MHz frequency has good separation from the 4 and 6 MHz harmonics of the pump waves. Thus, the informative signal can be filtered easily from the unwanted harmonics in the raw acoustic signal. In the case of the frequency ratio $d=1.32$ (when the maximum nonlinear wave amplitude is expected in $0.6 < d < 1.66$), the frequency separation becomes worse.

It is seen (Fig. 2b) that when the frequency ratio is 1, the inclination angles of both pump-wave sources are equal. This situation provides simplicity for the acoustical channel configuration; however, the frequency separation is lost here.

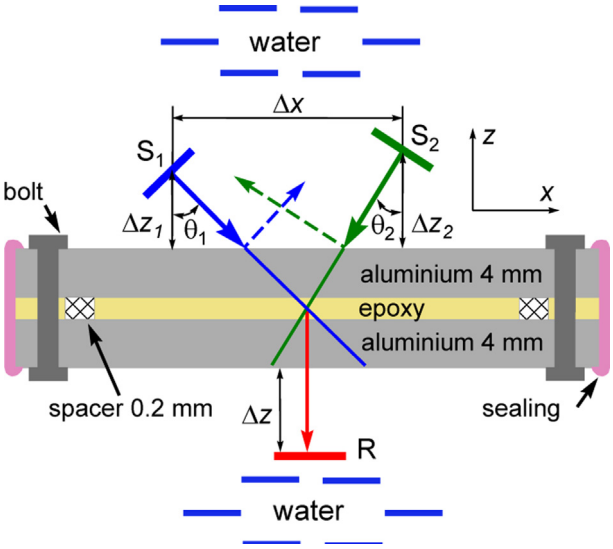

Fig. 3. Experimental arrangement of ultrasonic transducers for the non-collinear wave mixing in the through-transmission measurement mode. Dashed lines mark the specularly reflected pump waves. Not scaled.

3. Ultrasonic measurement setup

The SV(ω_1)+SV(ω_2)→L($\omega_1+\omega_2$) wave-mixing process is used to monitor the isothermal epoxy curing. An arrangement of ultrasonic transducers is shown in Fig. 3, for the immersion noncollinear wave-mixing measurements in the through-transmission mode.

The test parameters are listed in Table 2, with the following notations: f_1 and f_2 are frequencies of the pump waves generated by sources S_1 and S_2, respectively. N_1 and N_2 are the numbers of cycles of the used pump-wave generation. Inclination angles θ_1 and θ_2, as well as vertical offsets Δz_1 and Δz_2, respectively, are also related to the sources S_1 and S_2. The distance Δx between the pump-wave sources, as well as the distance Δz between receiver R and the specimen surface, is also shown in this figure.

Ten-millimeter-diameter planar broadband transducers are used for pump-wave generation. The receiver is a spherically focused broadband sensor having a 10 MHz central frequency. Acquired signals are amplified with a 20 dB preamplifier, digitized, and filtered using a narrowband filter (with a Kaiser window).

The peak-to-peak amplitude, energy, and change of the time-of-flight are used to parameterize the nonlinear wave signals. In an ideal case, the peak-to-peak amplitude and energy should give identical results. However, they may differ if the ultrasonic signal has a complex wave-shape. Previous studies [25], show that it is more practical to evaluate the energy of the nonlinear wave signals, as is done for the examples below.

Table 2
Parameters used for the non-collinear wave mixing experiments.

f_1, MHz	N_1, cycles	f_2, MHz	N_2, cycles	f_r, MHz	θ_1, deg	θ_2, deg	Δz_1, mm	Δz_2, mm	Δz, mm	Δx, mm
4	30	6	30	10	22	15.5	18	22	80	21

Arrangement of the transducers and specimen is chosen in a way that the central beams of the pump waves intersect in the epoxy layer (Fig. 3). Because of this arrangement and the finite beam width (which is of the same order as the transducer diameters), the following three volumes (where the nonlinear wave interactions occur simultaneously) can be separated:

1. In the upper aluminium layer, interaction of the pump waves occurs without any epoxy influence. Consequently, a constant amount of nonlinear wave energy is generated.
2. In the epoxy layer, the nonlinear wave is either not generated or very poorly generated, because the resonant conditions of the wave interaction are chosen for aluminium.

3. In the lower aluminium layer, the resulting amount of nonlinear wave energy is expected to depend strongly on the epoxy layer properties. Because of changes in the longitudinal and shear-wave velocities during the epoxy curing, transmission and refraction of the ultrasonic waves vary between the epoxy and aluminium interfaces. Hence, the resonant conditions of the wave interaction are not completely fulfilled here (i.e., generation of the nonlinear wave is ineffective). The amount of the generated wave energy also varies significantly in this volume, owing to changes in the acoustic properties of epoxy.

4. Ultrasonic monitoring of epoxy cure

The studied epoxy is a typical commercial system comprised of 3/4 Araldite® LY 1564SP resin and 1/4 XB 3486 hardener, by mass [26].

This mix is degassed for 20 min, spread on a 4 mm thick aluminium plate, and then covered with a second identical aluminium plate. Before this, to provide a uniform thickness for the epoxy layer, a 0.2 mm thick and 10 mm wide double-sided tape is placed along the plate perimeter. The whole "sandwich" is fixed with bolts, and its edges are sealed using a tacky "gum" to isolate the epoxy from water, as schematically illustrated in Fig. 3. These manipulations take about 10 min.

Then, the specimen is immediately placed in a water bath under an acoustic channel, and monitoring of the curing process is performed at 24.3 °C or at 40 °C, with a 30 s sampling rate.

As mentioned in Section 3 above, three parameters of the nonlinear ultrasonic signal are analyzed: the peak-to-peak amplitude, A_{pp}, energy, E, and change in the group time-of-flight, Δt. This last parameter is determined using the first measurement signal as the reference. For brevity, details of the chemical reactions during the epoxy cure are not discussed in the present paper; they can be obtained in the literature, e.g. [10,27,–29].

Test data for the 24.3 °C case are presented in Fig. 4a. They clearly show three characteristic points at 1.3 h, 6.7 h (10 h), and 20 h. The first peak at 1.3 h is well indicated by all three parameters. The minimum at 6.7 h is indicated by the peak-to-peak amplitude and energy. However, this peak is shifted at about 10 h in the time-of-flight curve.

Note that these ultrasonic measurements are performed in a large water bath, without a forced control of temperature, which changed slightly during the day-night cycle. This caused small "jumps" in the curves, seen (for example) in Fig. 4a between 25 h and 37 h. The results also show that the temperature variation does not influence the measurements when the epoxy-cure process is intensive, i.e., within 0–23 h interval.

Fig. 4a also shows a small deviation (different slopes) occurring between the peak-to-peak amplitude and energy curves within a 10–20 h interval. The third characteristic point (at about 20 h) is not easily seen in the energy and amplitude curves, but the time-of-flight curve shows a distinct phase change here. The energy and peak-to-peak amplitude show a trend toward becoming constant after passing this point. Also, the time-of-flight curve shows continuous ageing of epoxy after the change of phase at about 20 h.

Test data for the 40 °C case are presented in Fig. 4b. The curing process is accelerated by the higher temperature, in comparison with the 24.3 °C case. The initial linear decrease in the energy and amplitude is caused by a lower initial temperature of the specimen (which was brought from room temperature into heated water). Note that these ultrasonic measurements are performed in a small water bath with a forced control of temperature and magnetic stirrer. A cyclic variation of the temperature within a 0–5 h interval clearly shows the forced heating of the water bath when the temperature equilibrium is lost.

The following characteristic points can be derived from Fig. 4b: 0.3 h, 2.8 h (3.9 h) and 7.8 h. However, the first point (0.3 h) is not so well pronounced, if we compare it with the 24.3 °C case (1.3 h). This point is now seen only indirectly, as a local inflection of the curves.

Fig. 5 shows typical nonlinear ultrasonic signals (A_{pp}) at these characteristic points. The signals are scaled by the maximum amplitude measured at 20 h and 7.8 h for the T=24.3 °C and T=40 °C cases, respectively. As seen, the informative signal duration becomes shorter, thus indicating solidification of the epoxy.

5. DMA monitoring of epoxy cure

We performed an alternative isothermal cure characterization using an Anton Paar®MCR501 parallel plate rheometer. Similar equipment is widely used for this purpose—see, for example [30]—and its results can easily be interpreted in rheological terms (viscosity, damping, etc.).

First, a 26 mm diameter ring is mounted on the bottom plate of the rheometer and partially filled with a 3–4 mm epoxy layer (previously degassed during 20 min). Then, a 25 mm diameter top parallel plate is sunk into this ring until it contacts the epoxy. Since these preparations require a little more time compared to the ultrasonic tests, the delay before the test was about 15 min.

After closing a heating chamber around the specimen and setting the gained temperature (this takes other 5 min), we measured the shear viscosity at a 1 Hz frequency and a 1.8°

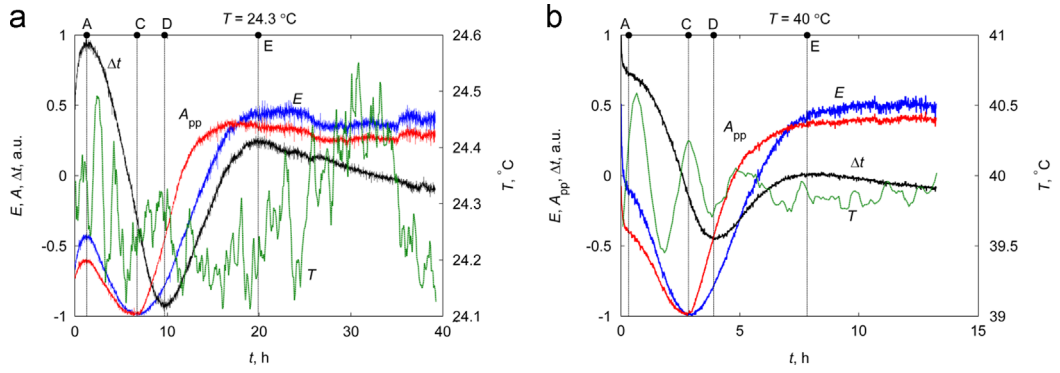

Fig. 4. Dynamics of the nonlinear ultrasonic signal parameters during the epoxy curing at 24.3 °C (a) and 40 °C (b). The parameters, except for the temperature, are scaled by their maxima and centered.

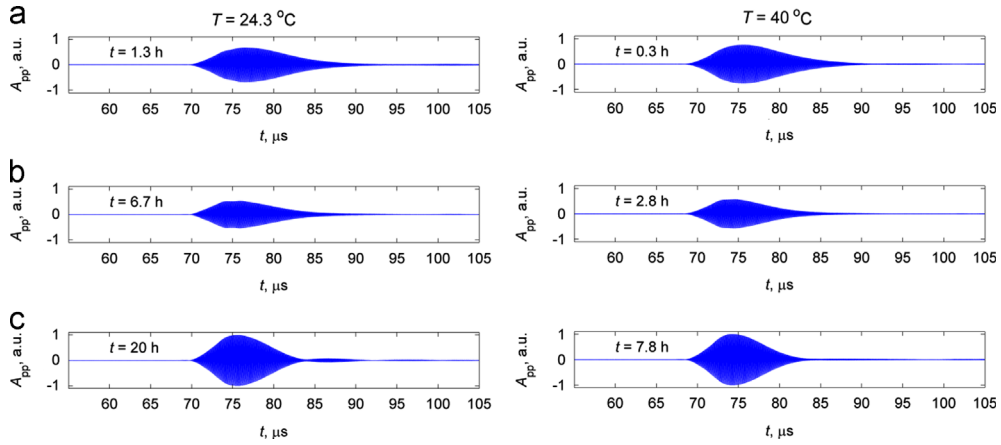

Fig. 5. Typical nonlinear ultrasonic signals during epoxy curing at 24.3 °C (left side) and 40 °C (right side): maximum viscosity (a), gel onset (b) and vitrification (c).

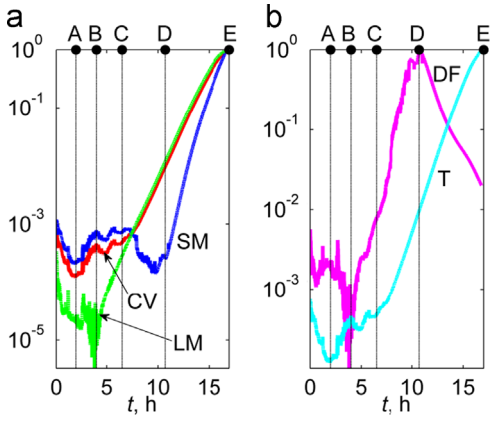

Fig. 6. Cure monitoring using DMA, 25 °C case. The data are log-scaled and normalized to their maximums. CV is the complex viscosity, SM is the storage modulus, LM is the loss modulus, DF is the damping factor and T is the torque.

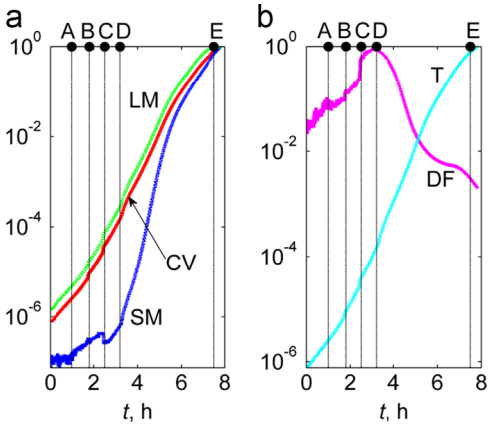

Fig. 7. Cure monitoring using DMA, 40 °C case. The data are log-scaled and normalized to their maximums. Notations are the same as in Fig. 6.

amplitude of rotational oscillations. Results are shown in Figs. 6 and 7 for the 25 °C and 40 °C cases, respectively. The following characteristic points and their physical backgrounds can be observed:

1. The first extremum, point A, corresponds to the minimal viscosity (as well as the storage modulus and torque). This obviously occurs not directly after mixing of the resin and hardener, but rather (due to inertia of the chemical processes) is postponed for some time: about 2 h at 25 °C. This roughly corresponds to 1.3 h noted above when discussing Fig. 4a, after the ultrasonic tests. This effect is almost invisible under the 40 °C test conditions, probably due to accelerated processes. Some minor inflections in the storage modulus and the damping factor curves are seen in Fig. 7 at about 1 h, but are difficult to interpret. In the ultrasonic tests discussed above, this effect also can be masked by a rapid decrease in the nonlinear wave amplitude, due to an increase in temperature within the measurement cell. Initial cell temperature was about 24 °C.
2. After a while, at point B (~4 h at 25 °C), the reaction rate seems to increase. This is seen as a minor local maximum of viscosity (and of the storage modulus, as well as torque) or a minimum of the loss modulus and damping factor (tan δ, which is a ratio of the loss and storage moduli), again for the 25 °C case only. Then the loss and storage moduli start to grow rapidly. Point B is not detected well for the 40 °C case, likely owing to the absence of any pronounced reaction-rate change in this case. Only barely visible "jumps" seen in Fig. 7 for the viscosity, torque, and loss modulus curves might potentially be attributed to point B.
3. The next extremum (point C) seems to be the onset of gelation; it occurs at about 7 h at 25 °C or 2.5 h at 40 °C. At this moment, the storage modulus starts to decrease locally, and the viscosity growth rate becomes yet higher (as well as that for the torque and damping factors). This feature corresponds well to the 6.7 h and 2.8 h points noted above when discussing Fig. 4 (ultrasonic tests). For the 40 °C case, only the storage-modulus decrease is seen well; the other changes (in the viscosity, torque, and damping) are barely visible in this case, obviously due to a quick transition to the next step in the material transformation.
4. The following extremum (point D) occurring at about 10–11 h at 25 °C or 3.2 h at 40 °C, is the peak of gelation and, therefore, of the damping factor as well, as adopted in ASTM D4473-90. Afterwards, the damping ability of the material rapidly vanishes. All other rheometry variables increase in magnitude, especially the storage modulus (representing the elastic portion of the stored energy). Point D is also visible in Fig. 4 (10 h or 3.9 h estimated for the 25 °C and 40 °C cases, respectively).
5. The last extremum is the onset of vitrification, point E, at about 17 h for 25 °C or 7–8 h for 40 °C. Rheometry is automatically stopped at this stage, due to exceeding the allowable torsional moment. When the specimens are then taken out of the machine, they appear completely solidified. This final point

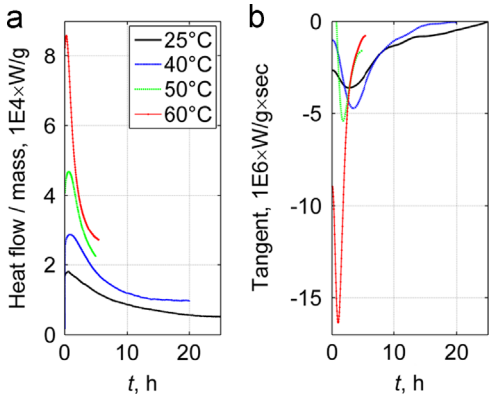

Fig. 8. Cure monitoring using DSC, at different temperatures. Heat flow (a) and its time derivative (b), normalized to the specimen mass.

also agrees well with the vitrification times derived from Fig. 4 (roughly 20 h or 7.8 h, respectively).

6. DSC monitoring of epoxy cure

Additional independent verification is performed with the isothermal calorimetric analysis, [31,32], using a Mettler Toledo® 882e apparatus. The specimens are 8–10 mg epoxy drops placed in standard aluminium cups, after a 20 min degassing. Two or three specimens are tested in each series, in the nitrogen atmosphere, at different temperatures ranging from 25 to 100 °C. A 10 °C/min rate is used at the initial heating stage (from the room temperature to the gained one). Then, the heat generated in the specimen by the curing reaction is recorded during a prescribed time.

Typical changes in the heat flow over time are presented in Fig. 8a. These curves clearly show only one point positioned at about 0.7 h (both for the 25 °C and 40 °C cases) or lefty for higher temperatures. According to the rheometry tests (Section 5), this point is hardly related to point A, which is positioned further to the right. However, it is logically possible that this exotherm peak is a precursor of the maximal viscosity.

Vitrification is shown by these curves (presumably when they approach the horizontal asymptote) at ~15 h or ~25 h. This, of course, differs substantially from the vitrification points derived above in the ultrasonic and rheometry tests; possible reasons for this discrepancy are discussed in Section 7.

Numerical derivatives of the curves (Fig. 8b), smoothed using 5th-order polynomials, reveal a little more information. First, there are minimums of the tangent, e.g., at about 3.3 h for both the 25 °C and 40 °C cases. The curves also show a change in slope at about 8–10 h or at 6–8 h for the 25 °C or 40 °C cases, respectively. As mentioned in Section 5, 10–11 h at 25 °C or 3.2 h at 40 °C is the peak of gelation (point D). However it is still not clear what can happen at 3.3 h for the 25 °C case.

7. Comparison of the test methods

The methods used in our study—nonlinear ultrasonics, DMA, and DSC—are compared in Table 3 according to their ability to detect the characteristic points of the epoxy cure. Of course, other methods such as dielectric tests [22,33,34] or magnetic resonance [33–35] could also be used and compared; however, the present study compares only the most common ones (DMA and DSC). All three methods are expected to characterize the epoxy from an uncured to completely cured state, in a single test. However, they have different sensitivities to the material properties, at least for the studied material and used equipment.

Table 3
Ability of the used test methods to detect characteristic points during the epoxy cure ("+" means ability, and "–" means disability; for the linear ultrasonics, data are taken from [5,15–19,34]).

Method	Max. viscosity, A	Gel onset, C	Gel peak, D	Vitrification, E
DSC	–	–	+	Barely visible
DMA	+	+	+	+
Linear ultrasonics	–	+	–	+
Nonlinear ultrasonics	+	+	+	+

DSC seems to show the lowest applicability to the epoxy-cure monitoring. First, it is not a surprise that the gelation point is only barely visible with DSC, since gelation does not significantly affect the heat flow [29]. However, it has a large impact on the mechanical response, as shown here by the DMA and nonlinear ultrasonic tests.

Although it should be revealed in DSC curves by a glass/rubber thermal transition, the vitrification point is also barely visible, because of the low reaction rate at the end of curing [29]. At the same time, the DMA and nonlinear ultrasonics reveal this point well, again due to a distinct mechanical background. The Temperature Modulated Differential Scanning Calorimetery (TMDSC) can provide better sensitivity for the vitrification [36], but this method is more complicated and still not widely used.

Comparison between DMA and nonlinear ultrasonics (which may in fact be considered as a contactless high-frequency DMA) favors nonlinear ultrasonics. First of all, it detects well (in Δt curve) the vitrification point in both tested cases (25 °C and 40 °C), whereas DMA is automatically stopped (because of a too thick gel) for the 25 °C case several hours before the vitrification.

The time point when the epoxy reaches the maximal viscosity is also seen more clearly in the nonlinear ultrasonic results, especially for the 25 °C case. Generally, the curves produced by the nonlinear ultrasonics are smoother than the DMA curves and are easier to analyze, due to their clear sinusoidal shapes and inflections.

The only constraint of the proposed method seems to be in its limited temperature range, since high-cure temperatures (say, over 50 °C) cause an extensive formation of bubbles in the water bath. However, this range can be extended somewhat by using some chemical additives for the water or even by employing another liquid as the coupling media. Ultimately, the tests can be performed even in air, using an air-coupled ultrasonic measurement technique. Also, it is possible to employ contact transducers for the wave mixing.

Last but not least, since both methods produce mechanical excitation in the specimens, concern might be raised about its effect on the test results. This is not applicable for the gelation point, because it has an isoconversion nature and thus is frequency independent [29]. However, the time of maximal viscosity may be accelerated, and the vitrification time may be either retarded (due to disturbed cross-linking) or accelerated (e.g., due to better diffusion of the hardener) [37,38]. The latter effect may be suspected of having occurred in the present tests (see Table 3). However, high-power ultrasonics (which could cause a cavitation) was not used here. Also, the ultrasonic sampling rate was low (once every 30 s), much lower than that in the performed DMA tests (every 1 s). At the same time, the effect of sonification (if any) is about the same as that of the low-frequency oscillations in DMA.

Table 4
Comparison of the characteristic points detected with the used methods.

	Max. visc., A		Gel onset, C		Gel peak, D		Vitrif., E	
Temperature *T*, °C	25	40	25	40	25	40	25	40
DSC, h	0.7	0.8	n/a	n/a	8–10	3.3	25	15
DMA, h	2	n/a	7	2.5	10–11	3.2	17	7–8
Nonlinear ultrasonics, h	1.3	0.3	6.7	2.8	10	3.9	20	7.8

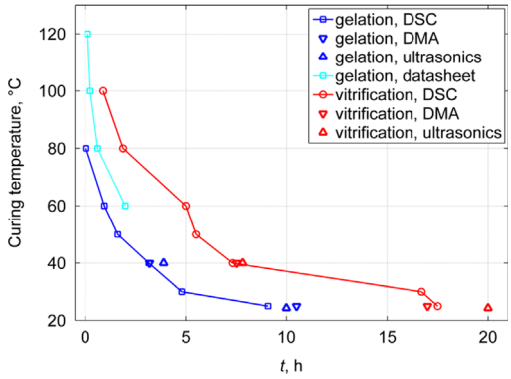

Fig. 9. TTT diagram for isothermal cure of LY 1564SP/XB 3486 epoxy.

Therefore, the observed discrepancy in the vitrification times (Table 4), should rather be attributed to differences in the physical backgrounds of the used test methods. It should also be noted again that no generally accepted criterion exists to define the gelation and vitrification points [29], especially in DSC. Because of this (and also because of the different effects measured with different methods) and depending on the temperature range, DSC can show these points earlier than DMA, or vice versa [27].

Outlining all the tested temperatures, a time–temperature-transformation (TTT) diagram is presented in Fig. 9 for the gelation and vitrification times, which are taken at characteristic points D and E, respectively. Naturally, these values shift to shorter times with increasing cure temperature. Inflection of the vitrification curve is not seen here; it likely occurs above 100 °C.

DSC data are quite close to DMA and nonlinear ultrasonic results in the 40 °C case. For a lower temperature (the 25 °C case), the discrepancy is larger and persists up to 2.5 h. This difference can also be caused by the slightly different temperatures of the epoxy cure (24.3 °C in the ultrasonic measurements and 25 °C in the DSC and DMA measurements).

The gel time is also represented in Fig. 9 by the manufacturer's data [26], shifted to the right compared to the measured gel time, possibly because of a slightly different criterion used to define this point.

8. Conclusions

An immersion nonlinear ultrasonic-measurement technique is presented in this study, with application to in situ cure monitoring of epoxy resins or similar materials. It is demonstrated that the nonlinear ultrasonics—based on a noncollinear wave mixing and detecting changes in the 2nd- and 3rd-order elastic constants—can be very sensitive to the material transformations inherent in the cure process. At the same time, some of these transformations can be barely visible using conventional linear ultrasonics, or DMA, or DSC techniques. The main results of our study are outlined as follows:

(1) Elastic wave mixing using the immersion method shows effective monitoring capabilities for the epoxy cure. This nonlinear ultrasonic technique enables a reliable detection of several characteristic points of the cure process, such as the time of maximal viscosity, gel time, and vitrification time.
(2) The ultrasonic test data agree well with the data obtained using a conventional DSC and parallel-plate DMA methods. Moreover, the nonlinear ultrasonics detect certain characteristic points more effectively than the other two methods.
(3) The following advantages can be achieved using the nonlinear ultrasonic technique presented here: wave-mode and frequency separations, elimination of a surrounding medium influence, steering (scanning) a scattered wave and controlling the intersection volume location, single-sided or double-sided measurements, and an effective detector mode (for example, no informative signal excitation until the material properties are homogenous).

Acknowledgments

Dr. Ir. Roy Visser and Mr. Bert Vos (University of Twente) are gratefully acknowledged for their help with DMA and DSC tests. This work was partially supported by the Director, Office of Energy Research, Office of Basic Energy Sciences, Engineering and Geosciences Division, of the U.S. Department of Energy under Contract No. DE-ACO2-05CH11231.

References

[1] Wang H, Cao B, Jen CK, Nguyen KT, Viens M. On-line ultrasonic monitoring of the injection molding process. Polym Eng Sci 1997;37(2):363–76.
[2] Ono Y, Whiteside BR, Brown EC, Kobayashi M, Cheng C-C, Jen C-K, et al. Real-time process monitoring of micromoulding using integrated ultrasonic sensors. Trans Inst Meas Control 2007;29(5):383–401.
[3] Pawelzyk P, Toledo ML, Willenbacher N. Ultrasonic in-line monitoring of styrene miniemulsion polymerization. Chem Eng J 2013;219:303–10.
[4] Demčenko A, Akkerman R, Nagy PB, Loendersloot R. Non-collinear wave mixing for non-linear ultrasonic detection of physical ageing in PVC. NDT & E Int 2012;49:34–9.
[5] Lindrose AM. Ultrasonic wave and moduli changes in a curing epoxy resin—Ultrasonic techniques are examined as a means for monitoring reaction extent and the development of solid-phase moduli in a curing epoxy. Exp Mech 1978;18(6):227–32.
[6] Rokhlin SI, Lewis K, Graff KF, Adler L. Real-time study of frequency dependence of attenuation and velocity of ultrasonic waves during the curing reaction of epoxy resin. J Acoust Soc Am 1986;79(6):1786–93.
[7] Freemantle RJ, Challis RE. Combined compression and shear wave ultrasonic measurements on curing adhesive. Meas Sci Technol 1998;9:1291–302.
[8] Dixon S, Edwards C, Palmer SB. A technique for accurate shear wave velocity measurements of thin epoxy resin samples using electromagnetic acoustic transducers (EMATs). Meas Sci Technol 2001;12(5):615–21.
[9] Winfree WP. Ultrasonic characterization of changes in viscoelastic properties during cure. Proc IEEE Ultrason Symp 1983;1:866–9.
[10] Frigione M, Maffezzoli A, Acierno D, Luprano VAM, Montagna G. Nondestructive and in-situ monitoring of mechanical properties buildup in epoxy adhesives for civil applications by propagation of ultrasonic waves. Polym Eng Scie 2000;40(3):656–64.
[11] Pindinelli C, Montagna G, Luprano VAM, Maffezzoli A. Network development during epoxy curing: experimental ultrasonic data and theoretical predictions. Macromol Symp 2002;180:73–88.
[12] Dixon S, Jaques D, Palmer SB. The development of shear and compression elastic moduli in curing epoxy adhesives measured using non-contact ultrasonic transducers. J Phys D: Appl Phys 2003;36:753–9.
[13] Dixon S, Jaques D, Palmer SB, Rowlands G. The measurement of shear and compression waves in curing epoxy adhesives using ultrasonic reflection and transmission techniques simultaneously. Meas Sci Technol 2004;15:939–47.
[14] Bohmeyer W, Lange K, Stark W, Teteris G. Application of ultrasonic cure monitoring of thermosets in research and production. Proc Comp NDT 2011.
[15] Bacri JC, Courdille JM, Dumas J, Rajaonarison R. Ultrasonic waves: A tool for gelation process measurements. J Phys Lett—Paris 1980;41(15):369–72.
[16] Yoon SS, Yu WJ, Kim HC. Phase transition of epoxy resin during isothermal curing monitored by ultrasonic velocity measurements. J Mater Sci Lett 1992;11:1392–4.
[17] Alig I, Nancke K, Johari GP. Relaxations in thermosets. XXVI. Ultrasonic studies of the temperature dependence of curing kinetics of diglycidyl ether of bisphenol-A with catalyst. J Polym Sci Part B: Polym Phys 1994;32(8):1465–74.

[18] Matsukawa M, Nagai I. Ultrasonic characterization of a polymerizing epoxy resin with imbalanced stoichiometry. J Acoust Soc Am 1996;99(4):2110–5.
[19] White SR, Mather PT, Smith MJ. Characterization of the cure-state of DGEBA-DDS epoxy using ultrasonic, dynamic mechanical, and thermal probes. Polym Eng Sci 2002;42(1):51–67.
[20] Mc Hugh J, Stark W, Doring J. Evaluation of the cure behaviour of epoxy resin using rheometric and ultrasonic techniques. In: Green RE (editor). Proceedings of Nondestructive Characterization of Materials XI (2003), Springer-Verlag; 2003, p. 651–658.
[21] Korneev VA, Demčenko A. Possible second-order nonlinear interactions of plane waves in an elastic solid. J Acoust Soc Am 2014;135(2):591–8.
[22] Shigue CY, Dos Santos RGS, Baldan CA, Ruppert-Filho E. Monitoring the epoxy curing by the dielectric thermal analysis method. IEEE Trans Appl Supercond 2004;14(2):1173–6.
[23] Demčenko A, Koissin V, Korneev VA. Noncollinear wave mixing for measurement dynamic processes in polymers: physical ageing in thermoplastics and epoxy cure. Ultrasonics 2014;54(2):685–93.
[24] Asay JR, Guenther AH. Ultrasonic studies of 1060 and 6061-T6 aluminum. J Appl Phys 1967;38(10):4086–8.
[25] Demčenko A, Ravanan M, Visser HA, Loendersloot R, Akkerman R. Investigation of PVC physical ageing in field test specimens using ultrasonic and dielectric measurements. In: Proceedings of the IEEE international ultrasonics Symposium; 2012, p. 1909–1912.
[26] Warm-curing epoxy system based on Araldite® LY 1564 SP / Hardener XB 3486/Hardener XB 3487. Huntsman datasheet; 2004.
[27] Lange J, Altmann N, Kelly CT, Halley PJ. Understanding vitrification during cure of epoxy resins using dynamic scanning calorimetry and rheological techniques. Polymer 2000;41:5949–55.
[28] Isothermal cure of an epoxy by Dynamic Mechanical Analysis. Application note. Perkin-Elmer™ Instruments; 2000.
[29] Bilyeu B, Brostow W, Menard KP. Separation of gelation from vitrification in curing of a fiber-reinforced epoxy composite. Polym Composite 2002;23:1111–9.
[30] O'Brien DJ, Mather PT, White SR. Viscoelastic properties of an epoxy resin during cure,. J Compos Mater 2001;35(10):883–904.
[31] Fava RA. Differential scanning calorimetry of epoxy resins. Polymer 1968;9:137–51.
[32] Sourour S, Kamal MR. Differential scanning calorimetry of epoxy cure: isothermal cure kinetics. Thermochim Acta 1976;14:41–59.
[33] Challis RE, Freemantle RJ, Cocker RP, Chadwick DL, Dare DJ, Martin C, et al. Ultrasonic measurements related to evolution of structure in curing epoxy resins. Plast Rubber Comp 2000;29:109–18.
[34] Challis RE, Unwin ME, Chadwick DL, Freemantle RJ, Partridge IK, Dare DJ, et al. Following network formation in an epoxy/amine system by ultrasound, dielectric, and nuclear magnetic resonance measurements: A comparative study. J Appl Polym Sci 2003;88:1665–75.
[35] LaPlante G, García-Naranjo JC, Balcom BJ. Real-time cure monitoring of an epoxy/polyamidoamine system with unilateral magnetic resonance. NDT & E Int 2011;44:329–34.
[36] Xua SX, Li Y, Feng YP. Temperature modulated differential scanning calorimetry: on system linearity and the effect of kinetic events on the observed sample specific heat. Thermochim Acta 2000;359:43–54.
[37] Price GJ. Recent developments in sonochemical polymerization. Ultrason Sonochem 2003;10:277–83.
[38] Sharma S, Luzinov I. Ultrasonic curing of one-part epoxy system. J Compos Mater 2011;45:2217–24.